UNIVERSIDAD CARLOS III DE MADRID.

ESCUELA POLITÉCNICA SUPERIOR.

THEORETICAL STUDY OF THE AERODYNAMICS OF DELTA WINGS

Bachelor Thesis

By

María Martínez Pascual

Leganés, June 2016

Department of Thermal and Fluids Engineering.

ESCUELA POLITÉCNICA SUPERIOR.

THEORETICAL STUDY OF THE AERODYNAMICS OF DELTA WINGS

Bachelor in Aerospace Engineering

Author

María Martínez Pascual

Supervisor

Francisco Javier Rodríguez Rodríguez

Leganés, June 2016

Acknowledgments

I gratefully acknowledge my tutor Javier, for having made possible the present project and for all the effort put into it. His enthusiasm for teaching and research has been an important key for the growth of my interest in aerodynamics. Thank your for this great opportunity of learning.

I am grateful to my family. I especially would like to acknowledge my parents, Mercedes and Luis, for the support given during this degree. Their encouragement has been a fundamental part of my success.

I would also like to thank you all my friends. In particular to Amaya and Blanca, to whom I can't even start to express how grateful I am. Thank them for their selfless help during this four years and for making them a great experience.

III

Abstract

The present project emerges to provide a further development to the numerical an theoretical study on the aerodynamics of delta wings.

The study is focused on the analysis of the rolling up of detached vortex sheets on the upper surface of a delta wing.

First, the problem is introduced, describing the geometry used for the simulations. Then, the numerical approach is explained, giving details on the construction of the sheet of vortices that model the primary vortices that are created above the wing. In this section, the application of Kutta-Joukowski condition is explained. Also the procedure followed to build the vortices that roll up above the wing is detailed.

Then, the results obtained, such as the variation of the pressure over the surface and the effect of the thickness of the wing, are described and discussed.

Finally, some limitations of the present study and further improvements are presented.

v

List of Figures

Contents

Chapter 1

Introduction

1.1 Technological relevance

In this project the main objective is to study the behavior of a delta-wing. The delta-wing is a wing configuration used in supersonic flight, which was started to being studied in the 1930s by Alexander Lippisch, in Germany.

The supersonic flight has its origins in the aerodynamics of the propeller. Researchers realized that the lift of the airfoils dropped as their drag increased when the flow around it reached a certain velocity (450 mph). This was the phenomenon which high-speed aircraft would face by the end of the 1930s, the aerodynamic 'compressibility' ([1]).

In 1934 John Stack was already thinking about a 'compressibility research airplane'. By that time, compressibility might have seemed a distant problem, as the world airspeed record was still far from the speed of sound, but it was not.

In 1935, Adolf Busemann proposed sweeping back the wing to reduce the drag associated with high-speed flight. But only in Germany his idea was started to be developed.

In April 1944, Anthony F. Martindale put a Mark XI Spitfire into a dive where the aircraft reached more that 620mph (0.92 Mach, been 1 for the speed of sound). The wings of the aircraft was slightly swept back due to the stresses suffered. This high-speed dive, among others, gave researchers a insight of the kind of challenges supersonic flight would bring ([2]).

In the fall of 1944, Robert T. Jones presented the concept of the sharply angled delta and swept wing as a means of delaying and minimizing transonic and supersonic drag.

By the time WWII was finished, a number of aircraft had broken up as pilot overstressed them trying to recover from high-speed dives approaching sonic velocities. Then both the USA and the URSS recognized the potential of this type of design for supersonic flight. The swept wing immediately went to the top of design priorities for high-speed flight, due to two main advantages: the leading edge of the wing remains behind the shock wave created by the nose of the aircraft and generates a huge vortex which delays the stalling conditions of the aircraft.

Lippisch was taken to USA, where he ended up working at Convair, a leading aircraft manufacturer of the United States. Designers of this company begin with a sharply swept back thin wing and gradually filled in the trailing edge until they arrived at the 60-degree delta platform. This led to a much thin section of the wing and low aspect ratio. Such changes made it necessary to increase the requirements of stiffness and rigidity. The ratio of fuselage length to wingspan also changed dramatically, giving the fuselage the necessity to get a streamlined shape, which, prior to stability augmentation and flight control, was plagued of dangerous instabilities.

By the 1980s only the Concorde and the Space Shuttle were using delta-wings. The Concorde was able to sustain a cruise speed of 2 Mach due to its delta wings ([3]). For the Space Shuttle, which had the ability to glide for thousands of miles when landing, delta wings provided the needed lift that rectangular wings were not able to achieve at high speeds and altitudes. The use of this configuration became obsolete due to a series of disadvantages.

Some of the disadvantages were that delta-wings require high speeds and long runways for landing and take-off, they are no longer stable at high angles of attack and they produce a huge drag when trying to keep plane level. However, though structural and aerodynamic advantages are obtained from this wing configuration, their main disadvantages were due to control issues. One problem was pitch up. As the aircraft approaches stall, the fluid detaches going inwards from the tips, moving forward the center of pressure, which leads the aircraft to pitch up abruptly. Another problem is cross-flow wind as it makes one of the vortices greater than the other one, starting the rolling of the aircraft. This may lead to inertial coupling. As the plane had a huge part of its mass concentrated on its fuselage, when it started rolling, control was lost.

Between the 1980s and 1990, delta-wing where incorporated in several aircraft, one of which is the Eurofighter. The appearance of the computer-controlled flight control systems called "fly-by-wire" has allow the designers to compensate for some of the poor control qualities of delta wings. Also the inclusion of canards mounted on the fuselage in front of the aircraft have contributed to this as they improve its stability and maneuverability. It seems that delta-wing, which seemed to be obsolete, has gained a new chance of life.

1.2 State of the art

Nowadays, delta wings appear is several aircraft, such as the Eurofighter thanks to the incorporation of the computer-controlled flight control systems, which allow to compensate for the poor control qualities of this wing configuration.

As it is explained in [4], the dominant aspect of a subsonic flow over a delta wing are the two vortex sheet that detach from the region near the highly swept leading edges. This happens due to the difference on pressure between the upper, where it is lower, and the bottom surface, where it is higher. Thus, the flow separates (S_1 on Figure 1.2.1) and rolls-up over the leading edge creating what is called the primary vortex. This vortex goes above the wing and inboard the leading edge, and the fluid adheres again to the surface of the wing at the primary attachment line (A_1), inducing an outward flow beneath of it. As the flow passes below the primary vortex, the boundary layer of the wing separates creating a secondary vortex rotating in the opposite sense to the main vortex, with its own separation (S_2) and attachment lines (A_2) , as it can be observed on Figure 1.2.1.
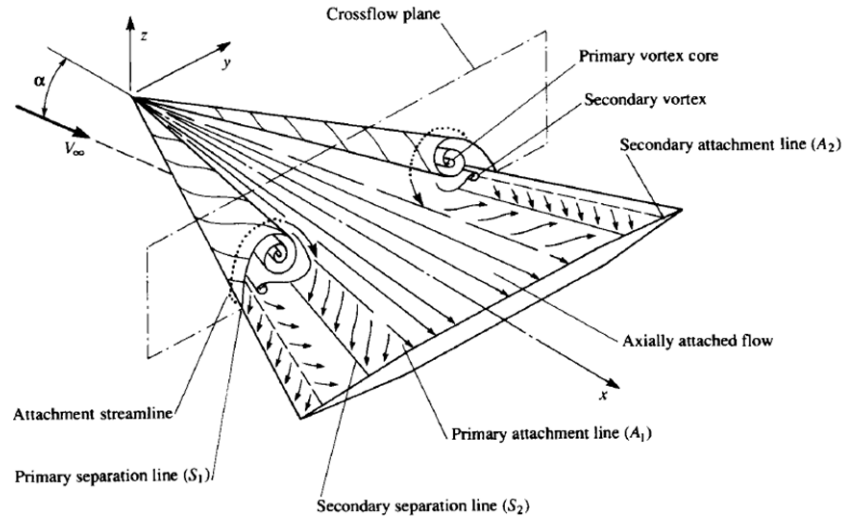
Figure 1.2.1: Schematic of the subsonic flow flied over the top of a delta wing at an angle of attack, from [4].

One of the main advantages of delta wings is that this two primary vortex provide stability to the wing and an increase in the lift. While the pressure at the bottom and on the middle of the upper surface is essentially constant, the accelerated fluid near the leading edge has as a consequence the drop on static pressure. This is what is seen on Figure 1.2.2, where the pressure distribution over the upper and lower surfaces of the wing is sketched, below the representation of the flat wing an the two primary vortices. Thereby, the vortex that is generated stays attached to the upper surface increasing the lift of the wing due to suction effect of the separation vortex, delaying the stalling conditions of the aircraft.
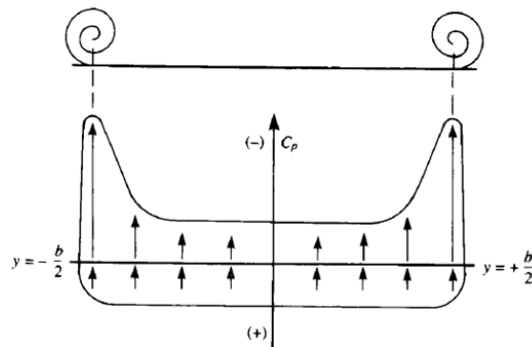
Figure 1.2.2: Schematic of the spanwise pressure coefficient distribution across a delta win, from [4].

Another huge advantage of the delta wing is that when flying at supersonic speeds, the leading edge of the wing remains behind the shock wave created by the nose of the aircraft. The consequence of this is that the component of the velocity normal to the leading edge is subsonic; the wing has a subsonic leading edge. This allows the aircraft to fly at higher speeds avoiding the increase on drag that may be produced by a rectangular wing, for example. The flow pattern at this conditions is therefore similar to the one shown on Figure 1.2.1.

1.3 Objectives

The main objective of this project is to develop a model for the study of the aerodynamics of the slender wings. In particular, the effect that the thickness of the wing has on the the rolling up sheet of vortices. Some of the inputs for the problems are going to be imposed such as the geometry of the wing and the initial position of the *nascent vortices* (what a nascent vortex is is defined in subsection 2.3.2).

From a more practical point of view, one of the aims of this project is to reproduce the evolution of the rolling up of the sheet of vortices that begins at the edges of the wing. At the beginning the problem is simplified as much as possible, so the initial configuration is a circle in a uniform flow. Then at each side of this circle, two vortices are located far enough from it, at a distance larger than the panel size but small compared to the span of the wing. They are called *detached vortices*. The sheet of vortices is created from the vortices that are generated at the edges of the profile. This vortices are called *attached vortices*. Their initial position is an input of the problem and their intensity is such that enforces the Kutta condition at the leading edges. As the attached vortices go further from the profile, they become detached vortices, and new vortices are generated. This is how the sheet of vortices develops and evolves with time.

At the end of this project it is expected to develop a computational tool that will be useful to obtained further more realistic results such as the influence of the side slip angle.

Chapter 2

Methodology

2.1 Definition of the problem

In this section the geometry of the problem is defined. Bare in mind that the problem is fully two-dimensional, so the computations are reduced to a single plane, the cross-flow plane (see Figure 1.2.1). The reference frame is set with the positive x-axis pointing downstream along the axis of symmetry of the wing, the y-axis following the spanwise direction and the z-axis perpendicular to the surface of the wing as it is illustrated in Figure 1.2.1).

The wing geometry can be described in very simple terms, as it is reduced to an ellipse which represents the transverse section of the wing. It is explained later that for simplicity the problem is made non-dimensional and the characteristic length is the mid span of the wing. Therefore the span of the wing goes from point (1, 0) to point (-1, 0) on the y-axis. These points are located at the right and left edges of the wing respectively. Is at this two points at the leading edge of the wing where the fluid leaves the surface generating the sheet of vortices. It is also at these points where the Kutta-Joukowski condition is applied. The shape of the upper part of the wing cross-section is given by the equation (2.1.1), and applying symmetry with respect to the horizontal axis, the lower surface is found. The cross-section of the airfoil is chosen to be symmetric also with respect to the vertical axis, although the code is actually able to handle non-symmetric geometries. The mid thickness of the wing (c) is taken as a 10% of the mid span of the wing (b).

$$\frac{z^2}{c^2} + \frac{y^2}{b^2} = 1 \tag{2.1.1}$$

For purposes that are explained later, the profile is discretized into k panels, separated by $m = k + 2$ nodes, and basic solutions are placed in the middle of each panels. The first and last nodes coincide with the point on the right side of the leading edge as it is indicated on Figure 2.1.1, where the approximate (as it may vary when obtaining the results) position of the nascent vortex is also shown. The number of the node increases counterclockwise.
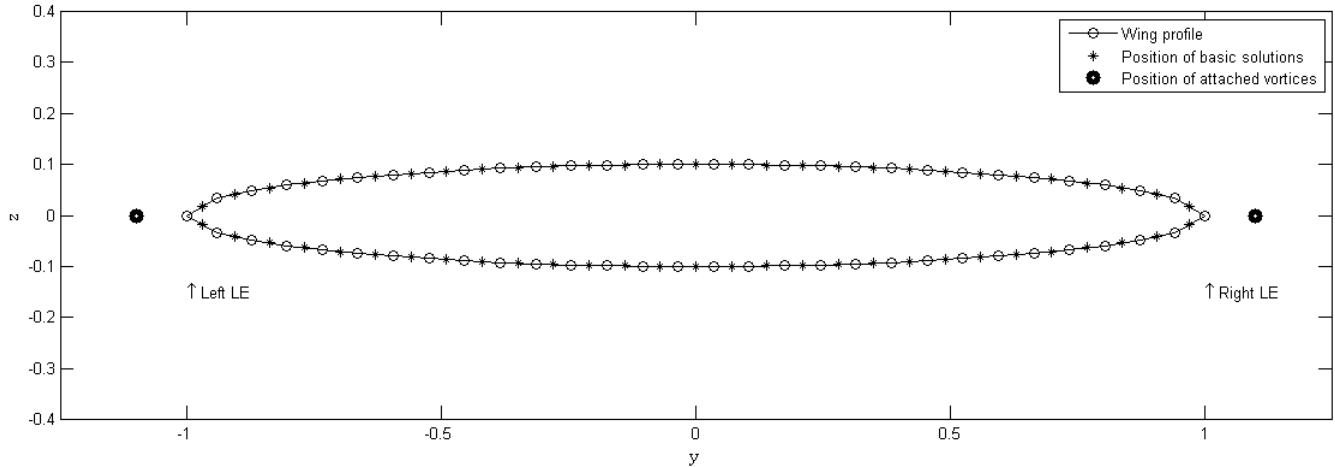
Figure 2.1.1: Scheme of the geometry

On each panel it is defined a normal vector ($\boldsymbol{n_k}$), pointing inwards the cross-section, and a tangent vector($\boldsymbol{t_k}$), pointing counterclockwise. Also, the middle point of the panel and the surface coordinate are defined, as it can be seen on Figure 2.1.2.
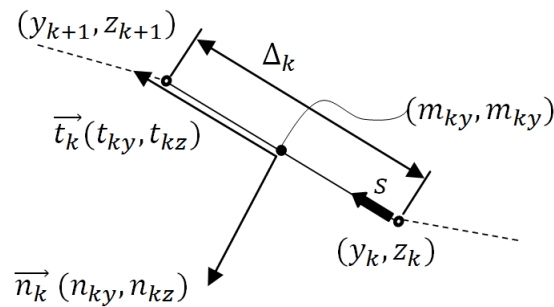
Figure 2.1.2: Definition of the middle point and normal and tangent vector associated to a panel.

Regarding the normal vectors used in future calculations, all of them are defined pointing outwards the domain Ω_C, as it is shown on Figure 2.1.3. In this Figure there are also defined the domains on which integrals are defined, although they may vary as the configuration of the problem does so, for instance, if we add more Kutta conditions or vortices.

Figure 2.1.3: Scheme of the problem to be solved numerically (nomenclature is described on sections 2.2 and 2.3).

2.2 General view

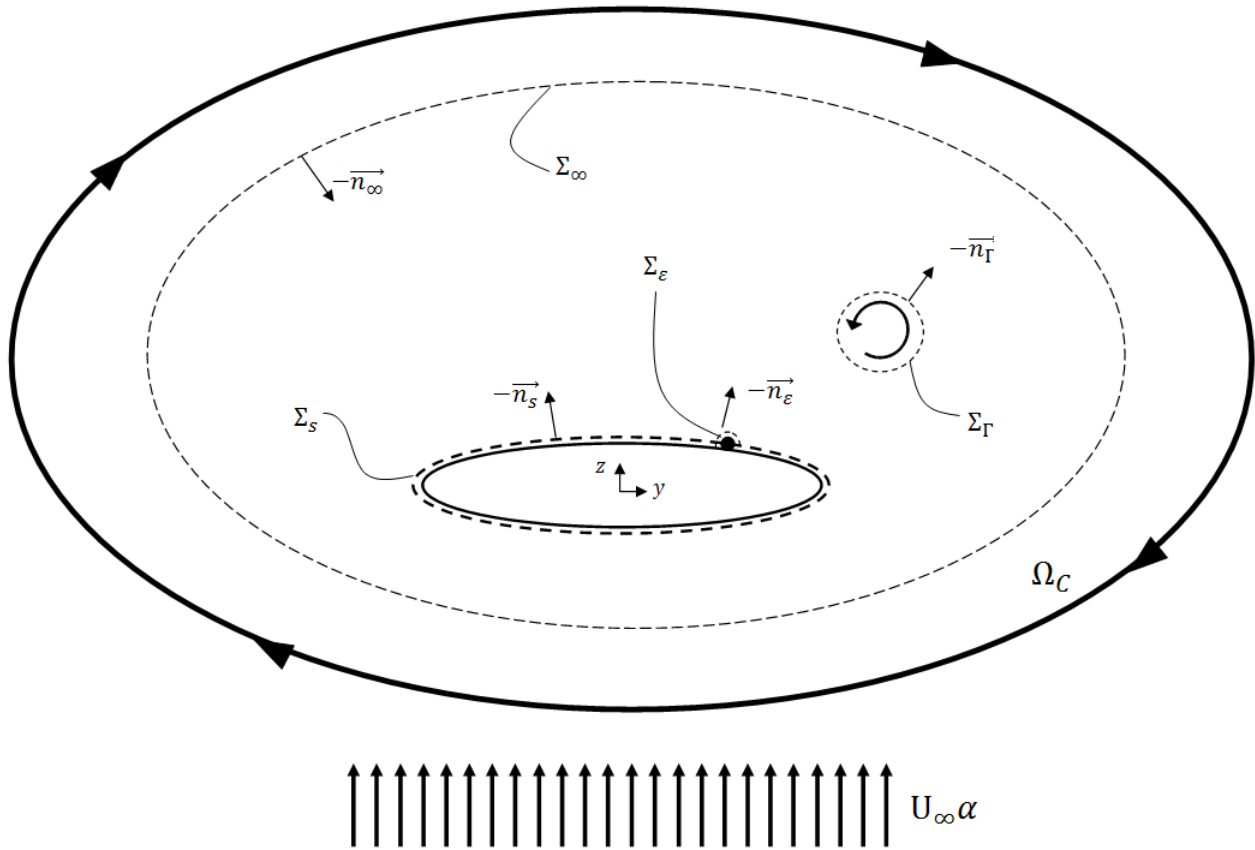As explained before, the computations to find the solution for the problem start with the simplest problem: a circle in a uniform flow. Then the circle is converted into an ellipse and two pair of vortices are positioned at each side near the leading edge. The pair of vortices that is further from the profile moves and gives way to other pair of vortices that is generated. In this way the sheet of vortices is build up.

The procedure followed to obtain the numeric solution is the one described in reference [5]. Therefore the problem to be solved is the following, which gives a solution for the potential flux (ϕ) around the body, assuming an incompressible fluid:

$$(\nabla^*)^2 \phi^* = 0$$
$$|\boldsymbol{x}^*| \to \infty, \phi^* \to U_\infty y^* \sin \alpha \cos \beta + U_\infty z^* \sin \beta \tag{2.2.1}$$

Where U_∞ is the free stream velocity and α and β are the angle of attack and the sideslip angle, respectively. The vector $\boldsymbol{x}^*$ defines a point at the surface of the wing (Σ_s) through which no permeability ($\boldsymbol{n} \cdot (\nabla^*) \phi^* = 0$) is assumed. Although at this point of the problem the Kutta-Joukowski condition is not necessary, it has to be mentioned as it will appear at some point of the development.

The problem, is made non-dimensional, using as characteristic scales of the longitude and the velocity the mid-span of the wing $(b/2)$ and the vertical velocity $(U_\infty \sin\alpha \approx U_\infty \alpha$, as the angle of attack is assumed to be small), respectively. So $\nabla^* = \dfrac{1}{(b/2)}(\nabla)$, $(\nabla^*)^2 = \dfrac{1}{(b/2)^2}\nabla^2$, $\phi^* = (U_\infty \alpha(b/2))\phi$ and $y^* = (b/2)y$. Therefore the problem to be solved is expressed as:

$$\nabla^2\phi = 0$$
$$|\boldsymbol{x}| \to \infty, \phi \to y\sin\alpha\cos\beta + z\sin\beta \tag{2.2.2}$$

The asterisk (*) stands for dimensional notation, and those variables without it are unitless, which are the ones used from now on. The problem is solved by the Green method, which expresses the potential at any point of the surface of the object as the superposition of a continuous distribution of two basic solutions. These are source $(G_j = \ln\|\boldsymbol{x}-\boldsymbol{x}_j\|)$ and doublets $(\boldsymbol{n} \cdot \nabla G_j)$, oriented to the outside of the object, as the vector normal to the surface.

2.3 Numerical Method

2.3.1 Flow around a circle and two vortices

As a first approach, the potential solution around a circle and two vortices is obtained. These vortices are referred as detached vortices. As they are far enough from the profile, they can be considered part of the far field potential. So the value of the potential at the infinity, expressed on equation (2.2.2), now includes the potential induced by the vortices:

$$|x| \to \infty, \phi \to y\sin\alpha\cos\beta + z\sin\beta + \sum_{i=1}^{N_{vor}} \frac{\Gamma_i}{2\pi}\theta \tag{2.3.1}$$

Where N_{vor} is the number of detached vortices, Γ_i the circulation of a vortex and θ is the angle between the horizontal axis and the vector that goes from the point (y,z), to the the point where the vortex is located. The circulation of the vortices is also non-dimensional so: $\Gamma = \dfrac{\Gamma^*}{U_\infty \alpha b/2}$.

It is known that the complex potential of sources and doublets satisfies the Laplace equation. So as $\nabla^2\phi = 0$ and $\nabla^2 G_j = 0$, the following identity is satisfied also:

$$G_j\nabla^2\phi - \phi\nabla^2 G_j = 0 \tag{2.3.2}$$

The Green function arises from applying the volume integral to the equation (2.3.2), extended to the domain defined as Ω_C. Within this domain a circular surface of radius $\varepsilon \ll 1$ is placed at the location of the basic solution of Laplace, to avoid the singularity. The Gauss theorem is then applied to this equation:

$$\int_{\Omega_C} (G_j\nabla^2\phi - \phi\nabla^2 G_j)dV = \int_{\Omega_C} \nabla \cdot (G_j\nabla\phi - \phi\nabla G_j)dV = \int_{\Sigma_C} (G_j\nabla\phi - \phi\nabla G_j) \cdot n\, d\sigma \tag{2.3.3}$$

The domain is expressed as $\Sigma_C = \Sigma_\infty \bigcup \Sigma_S \bigcup \Sigma_\varepsilon$ (all defined on Figure 2.1.3), where Σ_∞ includes the two vortices, which can be considered part of the far field. At this point it is convenient to substitute in equation (2.3.3)

the perturbed potential ($\phi^{'} = \phi - \phi_\infty$) as the integral over Σ_∞ disappears, leading to:

$$\int_{\Sigma_\infty \bigcup \Sigma_S \bigcup \Sigma_\varepsilon} (G_j \nabla \phi^{'} - \phi^{'} \nabla G_j) \cdot \boldsymbol{n} \, d\sigma = \int_{\Sigma_S \bigcup \Sigma_\varepsilon} [(G_j \nabla \phi - \phi \nabla G_j) - (G_j \nabla \phi_\infty - \phi_\infty \nabla G_j)] \cdot \boldsymbol{n} \, d\sigma = 0 \qquad (2.3.4)$$

The integral evaluated over Σ_S at the infinity is equal to zero. Knowing that $\boldsymbol{n} \cdot \nabla G_j = (-\boldsymbol{e}_r) \cdot (1/\varepsilon) \boldsymbol{e}_r$ and $G_j = \ln \varepsilon$:

$$\int_{\Sigma_\varepsilon} (G_j \nabla \phi_\infty - \phi_\infty \nabla G_j) \cdot \boldsymbol{n} \, d\sigma = \lim_{\varepsilon \to 0} \int_0^{2\pi} \left[(\ln \varepsilon) \nabla \phi_\infty \cdot \boldsymbol{n} + \phi_\infty \frac{1}{\varepsilon} \boldsymbol{n} \right] \varepsilon d\theta = 2\pi \phi_\infty(\boldsymbol{x}_j) \qquad (2.3.5)$$

To solve the rest of the integral over $\Sigma_s \bigcup \Sigma_\varepsilon$ we need to apply the condition of non-permeability ($\nabla \phi \cdot \boldsymbol{n} = 0$) at the surface of the circle:

$$\int_{\Sigma_\varepsilon \bigcup \Sigma_S} (G_j \nabla \phi - \phi \nabla G_j) \cdot \boldsymbol{n} \, d\sigma = \lim_{\varepsilon \to 0} \int_0^{\pi} \left[(\ln \varepsilon) \nabla \phi \cdot \boldsymbol{n} + \phi \frac{1}{\varepsilon} \boldsymbol{n} \right] \varepsilon d\theta + \int_{\Sigma_S} (-\phi \nabla G_j) \cdot \boldsymbol{n} \, d\sigma = \pi \phi(\boldsymbol{x}_j) - \int_{\Sigma_S} (\phi \nabla G_j) \cdot \boldsymbol{n} \, d\sigma$$
$$(2.3.6)$$

The solution to equation (2.3.4) is then:

$$\phi(y_j, z_j) = 2 \left[(m_{jy} \cos \beta + m_{jz} \sin \beta) + \sum_{i=1}^{N_{vor}} \frac{\Gamma_i}{2\pi} \arctan \frac{m_{jy} - y_{vi}}{m_{jz} - z_{vi}} \right] + \frac{1}{\pi} \int_{\Sigma_s} \phi(y, x) \frac{(\boldsymbol{x} - \boldsymbol{x}_j) \cdot \boldsymbol{n}}{|\boldsymbol{x} - \boldsymbol{x}_j|^2} ds \qquad (2.3.7)$$

Where $x_j = y_j \boldsymbol{j} + z_j \mathbf{k}$ is a fixed point at the surface of the object where the potential is calculated and $x = y \boldsymbol{j} + z \mathbf{k}$ is the vector-position of the integration variable in the surface integrals of equation (2.3.7).

As it has been anticipated at the beginning of this section, the Green method expresses that the potential at the point (y_j, z_j), $\phi(y_j, z_j)$ can be expressed as a superposition of the potentials of a continuous distribution of doublets oriented as the normal of the surfaces Σ_S and Σ_ε. For this reason, from equation (2.3.7), a numerical solution for the problem can be found. First, the geometry is discretized, divided into n panels. For each of the panels, the vector position of the adjacent nodes (r_k), the normal and tangent vectors (n_k, t_k), the middle point and the distance between them (m_n, Δ_n) and the distance between the nodes of the profile (Δ_k) can be calculated.

To find the numerical solution, the value of the potential along the panels has to be approximated to the value of the potential at the middle point. At this point, equation (2.3.7) can be rewritten as follows:

$$\phi(y_j, z_j) = 2 \left[(m_{jy} \cos \beta + m_{jz} \sin \beta) + \sum_{i=1}^{N_{vor}} \frac{\Gamma_i}{2\pi} \arctan \frac{m_{jy} - y_{vi}}{m_{jz} - z_{vi}} \right] + \frac{1}{\pi} \phi_k(y, z) \int_0^{\Delta_k} \frac{(\boldsymbol{x} - \boldsymbol{x}_j) \cdot \boldsymbol{n}_k}{|\boldsymbol{x} - \boldsymbol{x}_j|^2} ds \qquad (2.3.8)$$

Where s is defined as the surface coordinate and y_v and z_v are the vortex coordinates. Notice that the integral at the second term of equation is calculated for each panel. In case $k = j$ the integral is equal to zero, as $(\boldsymbol{x} - \boldsymbol{m}_j)$ is perpendicular to the normal vector of the panel. If $k \neq j$ the vector position can be expressed as $x = \boldsymbol{r}_k + s \boldsymbol{t}_k$, so:

$$\int_0^{\Delta_k} \frac{(\boldsymbol{x} - \boldsymbol{x}_j) \cdot \boldsymbol{n}_k}{|\boldsymbol{x} - \boldsymbol{x}_j|^2} ds = \int_0^{\Delta_k} \frac{(\boldsymbol{r}_k + s\boldsymbol{t}_k - \boldsymbol{m}_j) \cdot \boldsymbol{n}_k}{(\boldsymbol{r}_k + s\boldsymbol{t}_k - \boldsymbol{m}_j) \cdot (\boldsymbol{r}_k + s\boldsymbol{t}_k - \boldsymbol{m}_j)} ds = \frac{1}{((\boldsymbol{r}_k - \boldsymbol{m}_j) \cdot \boldsymbol{n}_k)^2} \int_0^{\Delta_k} \frac{(\boldsymbol{r}_k - \boldsymbol{m}_j) \cdot \boldsymbol{n}_k}{1 + \left(\frac{s + (\boldsymbol{r}_k - \boldsymbol{m}_j) \cdot \boldsymbol{t}_k}{(\boldsymbol{r}_k - \boldsymbol{m}_j) \cdot \boldsymbol{n}_k} \right)} ds =$$
$$\arctan \left(\frac{\Delta_k + (\boldsymbol{r}_k - \boldsymbol{m}_j) \cdot \boldsymbol{t}_k}{(\boldsymbol{r}_k - \boldsymbol{m}_j) \cdot \boldsymbol{n}_k} \right) - \arctan \left(\frac{(\boldsymbol{r}_k - \boldsymbol{m}_j) \cdot \boldsymbol{t}_k}{(\boldsymbol{r}_k - \boldsymbol{m}_j) \cdot \boldsymbol{n}_k} \right)$$
$$(2.3.9)$$

2.3.2   Kutta-Joukowski condition

Moving forward with the configuration of the problem, the arbitrary vortices that use to developed the equations in section 2.3.1 disappear. The aim now is to generate two symmetric vortices of unknown circulation (Γ_i) at a given location (t_{v1} and t_{v2}, see Figure 2.1.1), which will be referred to as nascent vortices.

Kutta-Joukowski condition determines the value of their circulation. Also it is known that the integral over the line C (equation 2.3.10) that encloses the profile (see Figure 2.1.3) is defined counterwise:

$$\Gamma = \oint_C \nabla\phi.dl \tag{2.3.10}$$

Kutta-Joukowski condition is applied at the points defined as the leading edge of the wing (Figure 2.1.1). At this points the fluid on the upper and the lower surfaces of the wing separate to rise the sheet of vortices. Therefore, the velocity of the fluid leaving the surfaces has to be equal in module and direction.

The circulation of the two vortices that want to be calculated are also unknown, so two more equations are needed. The application of the Kutta-Joukowski condition provides two new equations that allow the problem to be solved:

$$\frac{\phi_1 + \phi_{N+1}}{\Delta_{N+1}} = 0$$
$$\frac{\phi_{N/2} + \phi_{N/2+1}}{\Delta_{N/2+1}} = 0 \tag{2.3.11}$$

The problem of solving the potential over the profile reduces to a lineal system of *N+2* equations of the *N+2* unknowns $[\phi_1, \phi_2, ..., \phi_N, \Gamma_1, \Gamma_2]$:

$$\begin{cases} \sum_{k=1}^{N} R_{jk}\phi_k = 2\left[(m_{jy}\cos\beta + m_{jz}\sin\beta) + \sum_{i=1}^{N_{vor}} \frac{\Gamma_i}{2\pi}\arctan\frac{m_{jy} - y_{vi}}{m_{jz} - z_{vi}}\right] \\ \frac{\phi_1 + \phi_{N+1}}{\Delta_{N+1}} = 0 \\ \frac{\phi_{N/2} + \phi_{N/2+1}}{\Delta_{N/2+1}} = 0 \end{cases} \tag{2.3.12}$$

Where the coefficients are defined as:

$$R_{jk} = \left\{ \begin{array}{cc} \frac{1}{\pi}\left(\arctan\left[\frac{b_{jk}^t + \Delta_k}{b_{jk}^n}\right] - \arctan\left[\frac{b_{jk}^t}{b_{jk}^n}\right]\right) & k \neq j \\ 0 & k = j \end{array} \right\}, \tag{2.3.13}$$

with $b_{jk}^t = (\boldsymbol{r}_k - \boldsymbol{m}_j).\boldsymbol{t}_k$ and $b_{jk}^n = (\boldsymbol{r}_k - \boldsymbol{m}_j).\boldsymbol{n}_k$.

2.3.3   Velocity of a vortex

To go on with the problem, the nascent vortices have to move in time to shape the sheet of vortices. Time is made dimensionless, as the rest of the magnitudes of the problem, so: $t = \dfrac{t^*}{U_\infty\alpha(b/2)}$ .Once they move far enough from the surface of the wing they are called detached vortices.

The velocity of any particle of the fluid is the resultant of the addition o three contributions: the velocity induced by each of the panels of the profile, the velocity induced by the uniform flow and the velocity induced by any other vortex around (the vortex of which the velocity is been calculated does not induced velocity to itself).

The velocity induced by the profile on the vortex is obtained by derivating the result of integrating equation (2.3.2) over the surface (Σ_s), taking into account the condition of non-permeability ($\boldsymbol{n}\boldsymbol{.}(\nabla)\phi = 0$) at the surface:

$$\phi(y_v, z_v) = \int_{\Sigma_s} \phi \nabla G_j \cdot \boldsymbol{n} d\sigma = \int_{\Sigma_s} \phi \left(\frac{(\boldsymbol{x}{-}\boldsymbol{x}_j) \cdot \boldsymbol{n}_k}{|\boldsymbol{x}{-}\boldsymbol{x}_j|^2} \right) d\sigma \tag{2.3.14}$$

$$\phi(y_v, z_v) = \sum_{j=1}^{N} \phi_j \frac{\boldsymbol{n}_j \cdot (\boldsymbol{x} - \boldsymbol{m}_j)}{|\boldsymbol{x} - \boldsymbol{m}_j|^2} \Delta_j \tag{2.3.15}$$

$$\frac{\partial \phi}{\partial y} = \sum_{j=1}^{N} \phi_j \frac{\boldsymbol{n}_{ym}[(y - y_m)^2 + (z - z_m)^2] - [\boldsymbol{n}_{ym}(y - y_m) + \boldsymbol{n}_{zm}(z - z_m)] \cdot [2(y - y_m)]}{[(y - y_m)^2 + (z - z_m)^2]^2} \Delta_m \tag{2.3.16}$$

$$\frac{\partial \phi}{\partial z} = \sum_{j=1}^{N} \phi_j \frac{\boldsymbol{n}_{zm}[(y - y_m)^2 + (z - z_m)^2] - [\boldsymbol{n}_{ym}(y - y_m) + \boldsymbol{n}_{zm}(z - z_m)] \cdot [2(z - z_m)]}{[(y - y_m)^2 + (z - z_m)^2]^2} \Delta_m \tag{2.3.17}$$

These equations, (2.3.16) and (2.3.17), give the solution for the velocity induced by the body at any point of the space, outside the boundaries of the profile:

$$v = \frac{\partial \phi}{\partial y} - i \frac{\partial \phi}{\partial z} \tag{2.3.18}$$

To this velocity it is added the vertical contribution of the uniform flow, whose intensity is assumed to be equal to unity as the problem is non-dimensional:

$$v = \frac{\partial \phi}{\partial y} + i \left(1 - \frac{\partial \phi}{\partial z} \right) \tag{2.3.19}$$

Regarding the velocity that is induced by any other vortex in the domain it is calculated analytically. The analytical solution for the potential created by a vortex is derived with respect to the complex variable $t = y + iz$, and the velocity is obtained:

$$v_{v1 \rightarrow v2} = \overline{\frac{\partial}{\partial t} \left(\frac{-i\Gamma_1}{2\pi} \ln(t_2 - t_1) \right)} = \frac{i\Gamma_1}{2\pi} \frac{1}{\overline{t_2 - t_1}} \tag{2.3.20}$$

Therefore, the velocity of any vortex in the domain is:

$$v_v = \frac{\partial \phi}{\partial y} + i \left(1 + \frac{\partial \phi}{\partial z} \right) + \frac{i\Gamma_1}{2\pi} \frac{1}{\overline{t_2 - t_1}} \tag{2.3.21}$$

2.3.4 Building in the sheet of vortices

To build in the sheet of vortices, we start with a first pair of symmetric vortices that arise from the combination of the potential solution (equation 2.3.8) and the Kutta-Joukowski condition (equation 2.3.11). These vortices are

called *attached vortices* as they do not have velocity. The second pair of symmetric vortices appear at a certain distance, which is chosen to be greater than the panel size, from these two. They are the ones that have been refereed before as nascent vortices. As these vortices evolve with time they become part of the detached vortices that shape the sheet of vortices. Once the pair of vortices is far enough from the profile, a new pair of symmetric vortices appear in between them and the attached vortices..

Figure 2.3.1 shows a simple scheme of how the sheet of vortices is created. At $t = 0$, the configuration includes the attached vortices $(\Gamma_{fv1}, t_{fv1}, \Gamma_{fv2}, t_{fv2})$ and the first pair of moving vortices $(\Gamma_{v1}, t_{v1}, \Gamma_{v2}, t_{v2})$. When the time is set up, the velocity of these vortices is calculated (t'_{v1}, t'_{v2}) and the potential on each panel (ϕ_k) is recalculated accounting for the potential generated at the new positions. Once these vortices are far enough from the fixed vortices, a new pair of vortices is generated in between the fixed and the moving existing vortices and the potential of the panels and the circulations and positions of these new vortices $(\Gamma_{vi}, t_{vi}, \Gamma_{vi+1}, t_{vi+1})$ are calculated. The condition for the generation of a new vortex depends on a numerical parameter that is set arbitrarily (D_{min}) as explained later. The velocity of all the moving vortices is calculated again and new vortices appear under the same condition. This loop goes on until the time of calculation finishes.
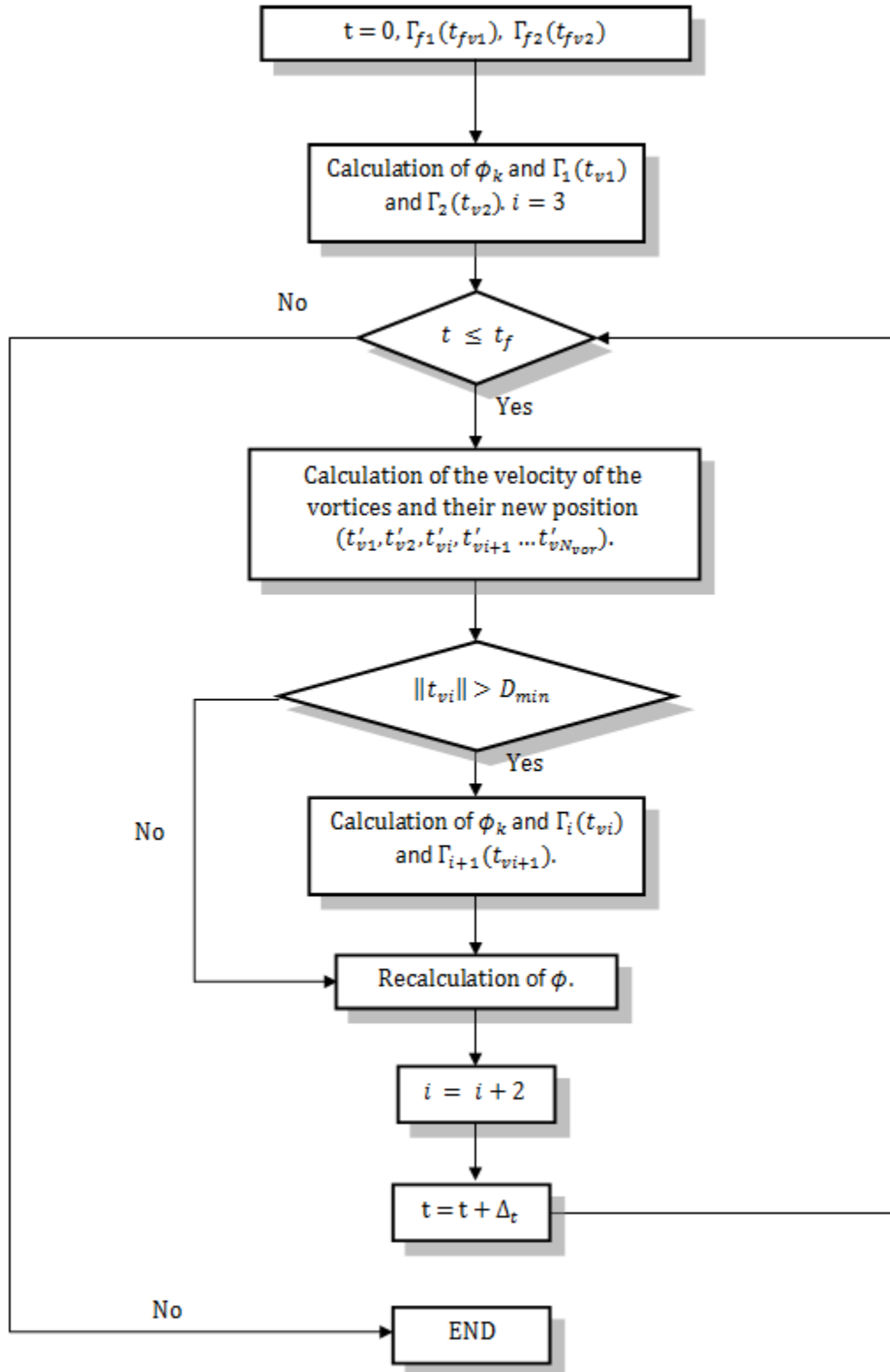
Figure 2.3.1: Flowchart of the generation of the sheet of vortices.

Chapter 3

Validation

3.1 Flow around a cylinder and two vortices

The first thing done in order to check if the results given by the code are correct is to find the potential flow of the simple case of a circle and two vortices submerged in a uniform flow going on the vertical direction. The analytic functions that represent an uniform flow and a vortex are elementary solutions of the Laplace equation (2.2.2). To find the theoretical solution to this problem, *Milne-Thompson theorem* is applied to a flow field composed of these to elementary solutions: an uniform flow, going in the positive direction of the z-axis, and two vortices. The potential of this flow is obtained from equation (3.1.1).

$$f = -iU_\infty \alpha t - \frac{\Gamma_{v1}^*}{2\pi} \ln(t - t_{v1}) - \frac{\Gamma_{v2}^*}{2\pi} \ln(t - t_{v2}) \qquad (3.1.1)$$

As for the numerical solution, the equation for the potential of an uniform vertical flow and two vortices is made non-dimensional, with the same characteristic scales used for the numerical problem:

$$f = -it - \frac{\Gamma_{v1}}{2\pi} \ln(t - t_{v1}) - \frac{\Gamma_{v2}}{2\pi} \ln(t - t_{v2}) \qquad (3.1.2)$$

.

The *Milne-Thompson* circle theorem is a statement that gives a new streamfunction for a fluid flow when a circle is placed on it. Let $w = f(t)$ be a complex streamfunction with no rigid boundaries and no singularities within $|z| = a$. If a cylinder $|z| = a$ is placed into that flow, the complex potential for the new flow is given by:

$$w = f(t) + \overline{f\left(\frac{1}{\overline{t}}\right)} = f(t) + \overline{f}\left(\frac{1}{t}\right) \qquad (3.1.3)$$

Therefore, the analytical solution for this problem is obtained by means of known basic solutions of potential theory to which Milne-Thompson theorem is applied, giving the following expression:

$$w = -it + i\frac{1}{t} - \frac{i\Gamma_{v1}}{2\pi}\left[\ln(t - t_{v1}) - \ln\left(\frac{1}{t} - \overline{t_{v1}}\right)\right] - \frac{i\Gamma_{v2}}{2\pi}\left[\ln(t - t_{v2}) - \ln\left(\frac{1}{t} - \overline{t_{v2}}\right)\right] \qquad (3.1.4)$$

The analytical value of the potential is calculated on the surface of the body, where equation (2.3.8) gives the numerical solution. The error between these two solutions is shown in Figure (3.1.1) and it is obtained by equation

15

(3.1.5).

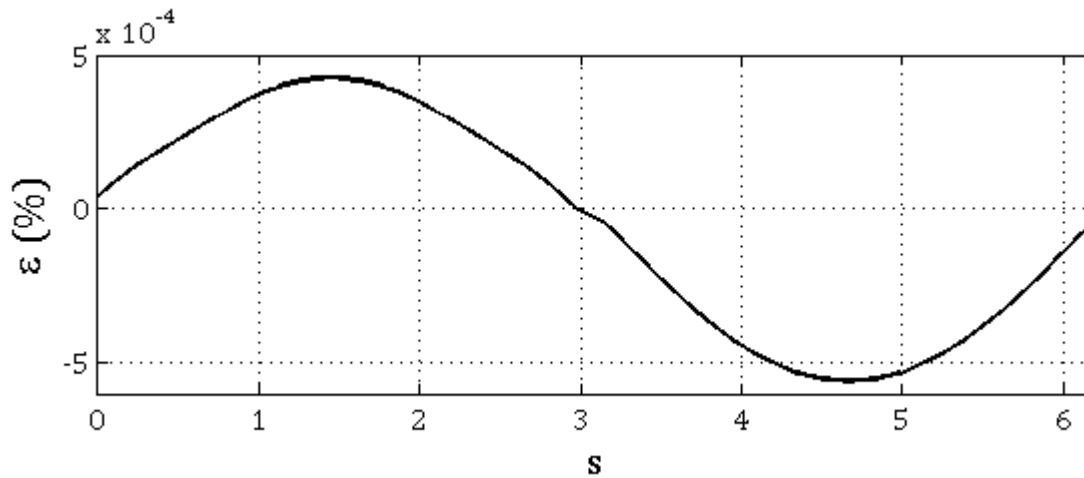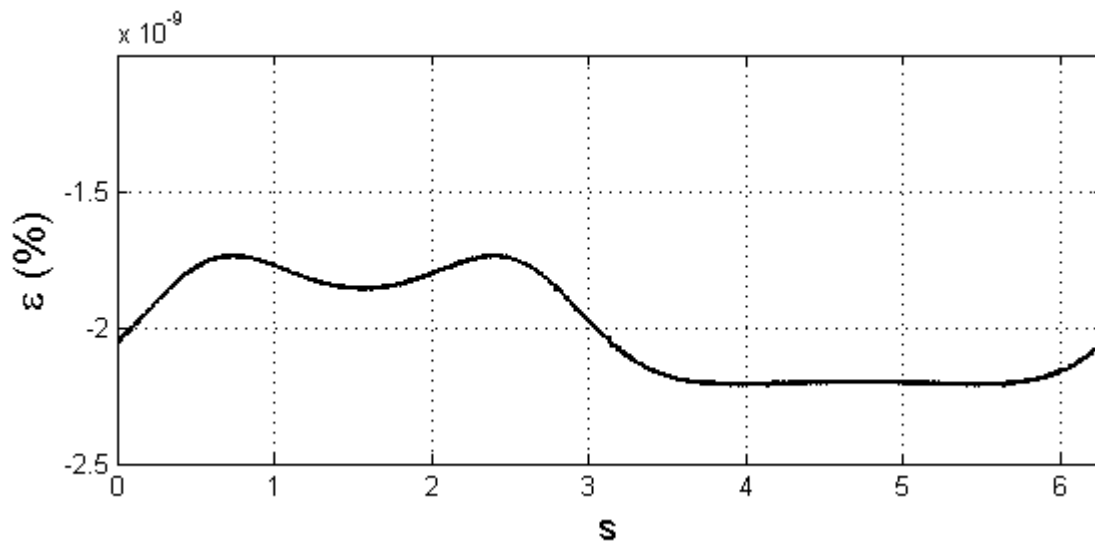$$\varepsilon = \frac{\phi - w}{w} \qquad\qquad (3.1.5)$$

(a) Error between analytical and numerical solutions of the potential for m = 40.

(b) Error between analytical and numerical solutions of the potential for m = 400.

Figure 3.1.1: Error between analytical and numerical solutions of the potential as a function of s, the coordinate along the surface of the profile.

The fist thing that is noticed is the non-symmetric distribution of the potential. This is due to the potential induced by the vortices, which break the symmetry with respect to the horizontal plane.

The graphs show the error between analytical and numerical solutions for the same geometry but with different number of panels. The configuration used in Figure 3.1.1a has a number of panels equal to the 10% of the number of panels of Figure 3.1.1b. Then it can be said that even if the number of panels is small, the error is

reasonable, taking into account that the numerical scheme used is a second order method, since it stays below an order of magnitude of 10^{-2}.

3.2 Pressure distribution

The linearized potential theory, explained on [6] predicts an infinite suction peak at the leading edges of the wing on its pressure distribution (see Figure 3.2.1). According to this theory, and adapting equations on [6] to the present problem, vertical ($w(y, z, 0^{\pm})$) and horizontal ($u(y, z, 0^{\pm})$) velocities on the surface of the wing are calculated by means of equation 3.2.1.

$$u\left(y, z, 0^{\pm}\right) + iw\left(y, z, 0^{\pm}\right) = \mp \frac{U_{\infty} \alpha y}{\sqrt{\left[\dfrac{b}{2}\right]^2 - y^2}} - iU_{\infty} \alpha \tag{3.2.1}$$

$$u\left(y, z, 0^{\pm}\right) + iw\left(y, z, 0^{\pm}\right) = \mp \frac{y}{\sqrt{\left[\dfrac{b}{2}\right]^2 - y^2}} - i \tag{3.2.2}$$
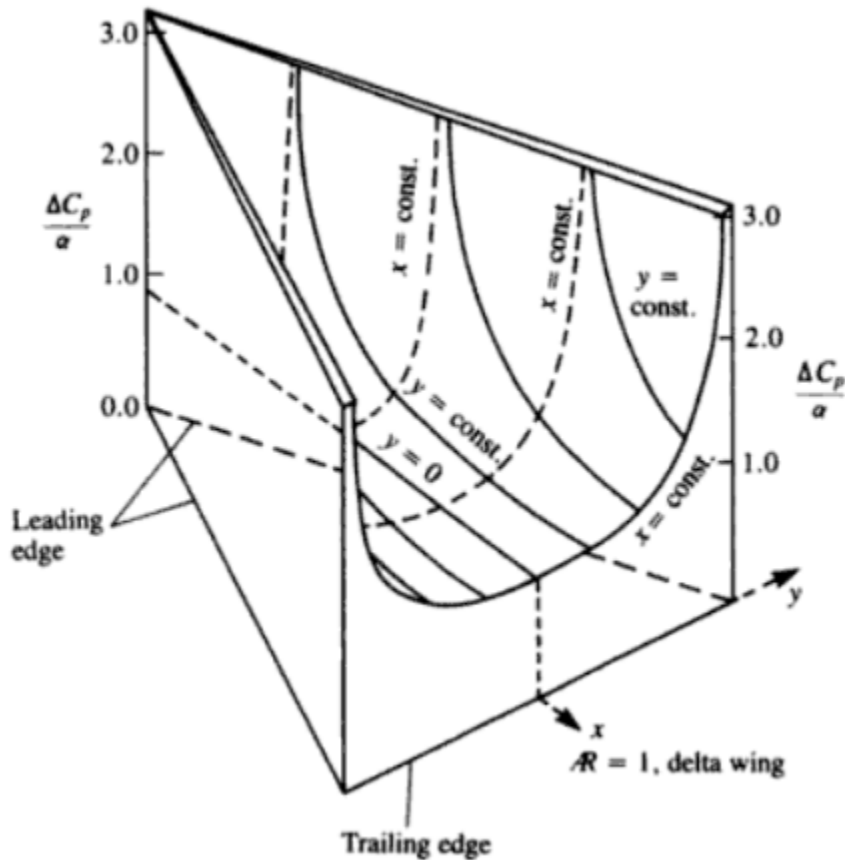
Figure 3.2.1: Pressure difference distribution on a slender delta wing predicted by linearized theory [6].

Which made non-dimensional would look as equation 3.2.2. This equation gives the values of the velocity of the fluid at each point on the surface of the wing. The numerical solution is obtained by making the wing extremely thin ($c = 0.005b$) and calculating the velocity on the surface of the wing at an instant where the vortex sheet is stable ($t = 1$, for standard conditions that are defined on Subsection 4.1, except for the value of the thickness). Analytical and numerical solutions are shown together in Figure 3.2.2. On it can be seen that numerical solution for the pressure coefficient difference has has very high values at the leading edges of the wing. Based on this, numerical solution can be considered a good approximation, taking into account that is not obtained over a flat plate as the analytical solution.
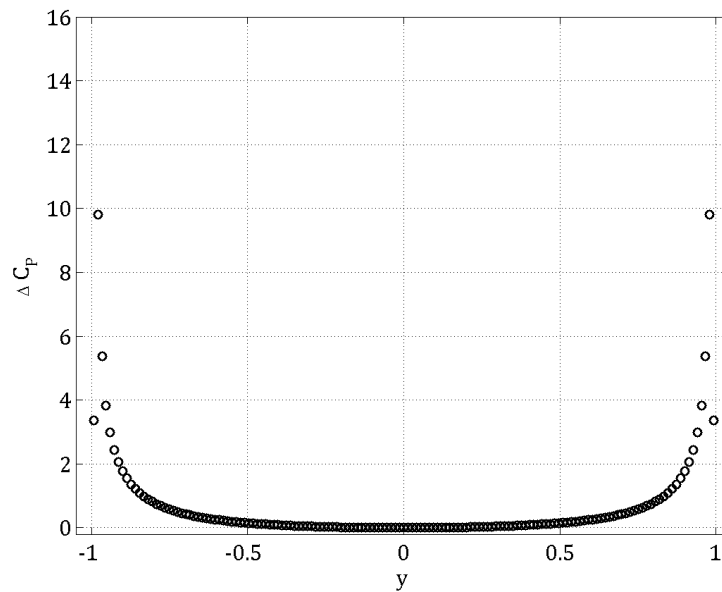
Figure 3.2.2: Numerical and analytical solutions for pressure distribution.

Chapter 4

Results

The aerodynamics of a delta wing are going to be studied. To do so, equations (2.3.8) and (2.3.11) are combined to form a system of $k+2$ equations, as the one shown on equation (2.3.12). This system gives the solution for the potential at each panel of the discretized geometry (ϕ_k) and the circulation of the vortices that shape the sheet of vortices (Γ_i).

The sheet of vortices grows from the separated flow at the leading edge of the wing. The first vortex is fixed, so that it has no velocity and it sets the origin of the sheet of vortices. It is positioned at an arbitrary distance (d_{att}, see Figure 4.0.1) from the leading edge, as it was shown on Figure 2.1.1. The fixed vortex is the attached vortex that appeared in section 2.3.4. The second vortex of the sheet is the first moving vortex as it also placed at a given distance (d_{mov}) from the attached vortex. The vortices that are created after this first moving vortex are positioned in between the attached vortex and the closest moving one.
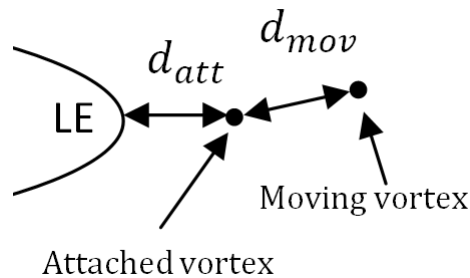

Figure 4.0.1: Schematic representation of the initial positions of the attached vortex and first moving vortex of the sheet.

4.1 Numerical parameters

The effects of the variations of the numerical magnitudes are studied in this section. All the simulations carried out are done using the circulation line simplification, explained on on the following section, 4.2. These numerical parameters are the following:
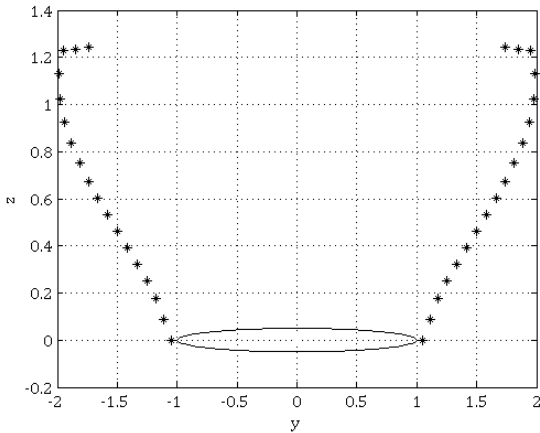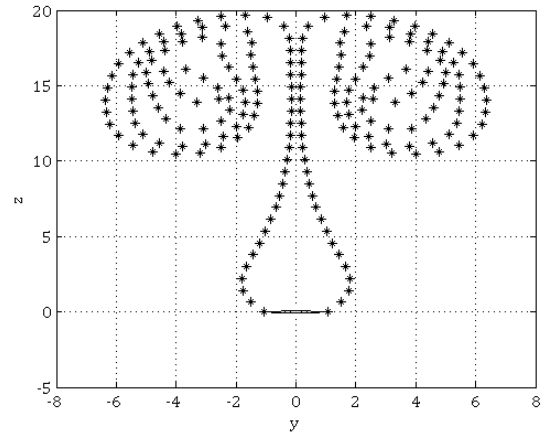
- d_{att} - The distance of the attached vortex.

- d_{mov} - The distance of first moving vortex.

- d_v - The minimum distance between the attached vortex and the closest moving vortex to generate another vortex.

- D_{min} - The radius to construct the line of circulation.

The first magnitude is the distance of the attached vortex with the leading edge of the wing (d_{att}), which goes only in the y-direction. This attached vortex provides stability to the method, it has no velocity and is placed very close to the leading edge. This parameter has a small approximated range of possible values. If the vortex is placed very close to the leading edge of the wing, numerical calculation does not hold. If the vortex is placed too far, the results do not give a good approximation of the actual solution of the flow, though high values are safer for the stability of the method.

To get approximate ranges for this value, specially to know which is the minimum allowed, different simulations are carried out for given conditions of time ($\Delta_t = 0.01, t = 3$) and geometry ($b = 1, c = 0.05$). The tested ranges of values within the code gives an acceptable solution are: for m = 200, [0.00001, 2], for m = 400, [0.01, 2] and for m = 800, [0.01, 2]. It it worth to mention that values above the maximums of these ranges can be afforded numerically, but the results would be further from reality. Also, longer distances delay the rolling up of the sheet of vortices.

The second numerical magnitude if the distance of the first moving vortex to the attached vortex (d_{mov}), which is a vector with components different from zero in both axis of symmetry. Simulations to investigate the possible range for this distance are done for the same three values of m, under the same conditions of time and geometry as for the distance of the attached vortex and fixing $d_{att} = 0.05$. It is observed that the distance on the y-axis may be chosen from a range of values of [0.0001, 2] without concerning much about it since it has not a great influence on the results. However, if the distance on the z-axis exceeds a determined order of magnitude (10^{-3} for m = 200, 400, 600 and 800) numerical analysis does not give the expected solution as is is seen in Figure 4.1.1b.

These two distances d_{att} and d_{mov} have to be adjust together. This means that having a possible physical solution of the fluid if one of them is changed this solution may vary giving a non-valid solution. Figure 4.1.1 shows how the shape of the vortices change by increasing the vertical component of d_{mov} in one order of magnitude.

(a) Sheet of vortices at $t = 1$ for $d_{mov} = 0.5 + i0.005$ (b) Sheet of vortices at $t = 1$ for $d_{mov} = 0.5 + i0.05$

Figure 4.1.1: Primary vortices generated for $d_{att} = 0.05$ for different values of d_{mov}.

Other numerical magnitude that is set arbitrarily is the minimum distance required (d_v) between the attached vortex and the closest moving vortex to generate a new vortex. To find an approximate criteria to establish this value relating it to the geometry of the wing, several simulations are carried out under the same conditions of time ($\Delta_t = 0.01, t = 6$) and geometry ($b = 1, c = 0.05, d_{att} = 0.05, d_{mov} = 0.5 + i0.0001$). These simulations consist in changing the value of the distance to get the closest solution to the time just before the vortex breaks, meaning the sheet crosses itself or changes direction drastically. Table 4.1.1 shows the relation of the minimum distance required between the vortices and the panel size by means of a coefficient ($a = d_v/D$), for geometries with different number of nodes. Figures 4.1.2, 4.1.3, 4.1.4 and 4.1.5 show how the vortices behave for the different cases gathered on table 4.1.1.

	$m = 200, D = 0.0203$		$m = 400, D = 0.0101$		$m = 600, D = 0.0067$		$m = 800, D = 0.005$	
d_v	0.0913	0.1014	0.0858	0.0908	0.0874	0.0907	0.0856	0.0881
a	4.5	5	8.5	9	13	13.5	17	17.5

Table 4.1.1: Relation ($a = d_v/D$) between the size of the panel (D) and the distance from the attached vortex to the moving one (d_v).

(a) For $a = 4.5$.

(b) For $a = 5$.
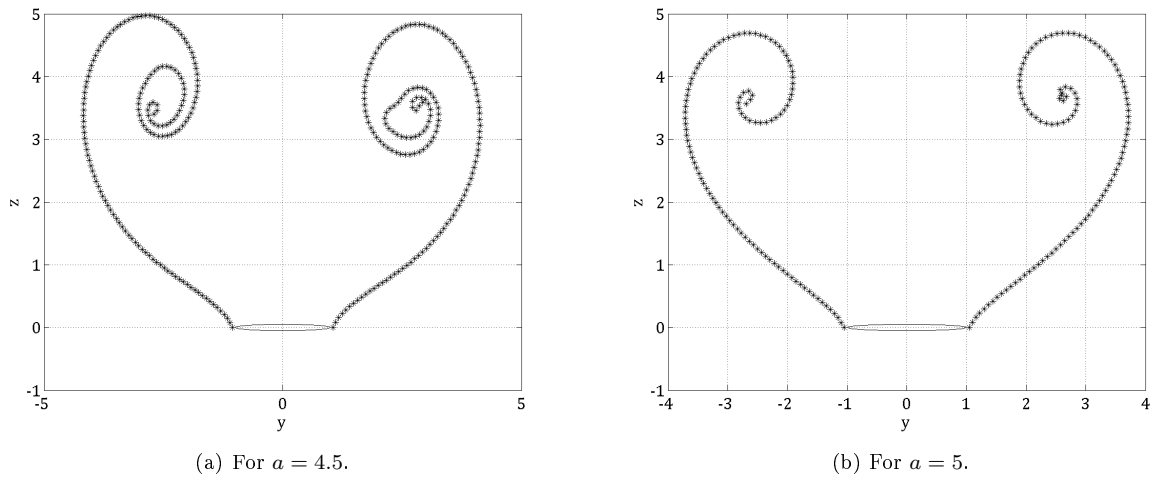
Figure 4.1.2: Shape of the sheet of vortices for $m = 200$ at $t = 6$.

(a) For $a = 8.5$.

(b) For $a = 9$.
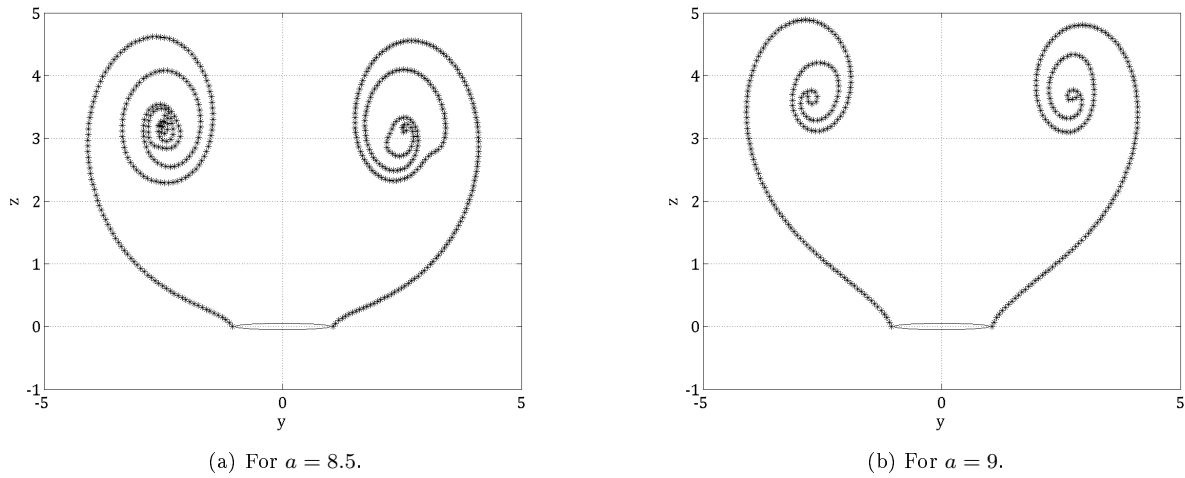
Figure 4.1.3: Shape of the sheet of vortices for $m = 400$ at $t = 6$.

(a) For $a = 13$.

(b) For $a = 13.5$.
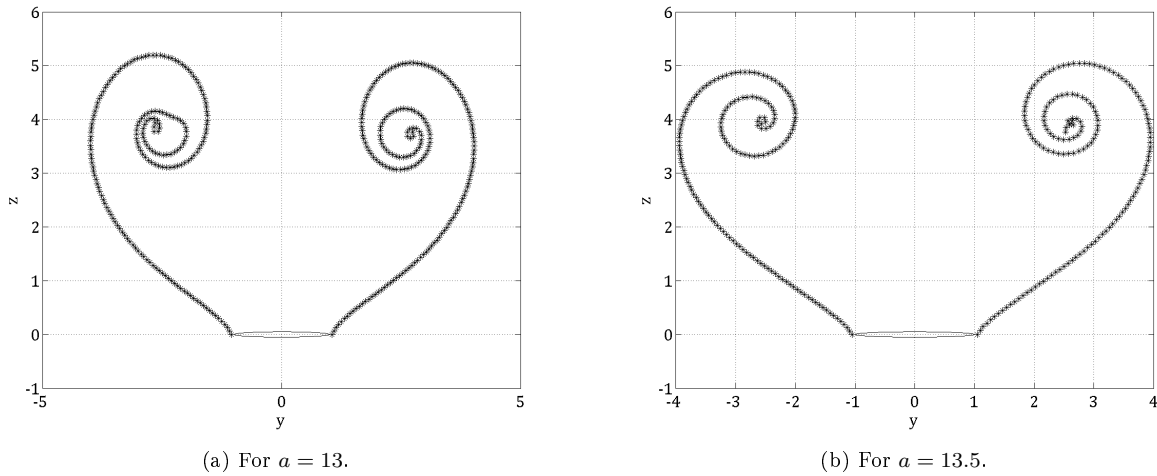
Figure 4.1.4: Shape of the sheet of vortices for $m = 600$ at $t = 6$.

(a) For $a = 17$.

(b) For $a = 13.5$.
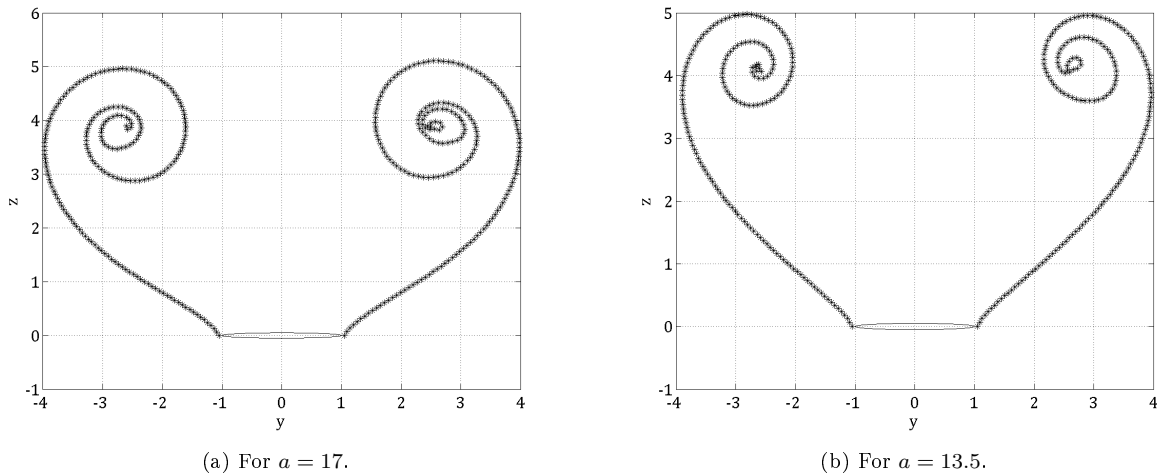
Figure 4.1.5: Shape of the sheet of vortices for $m = 800$ at $t = 6$.

A linear interpolation between can be done to obtain an approximation of the coefficient a needed as a function of the number of nodes of the profile (m). According to the values of Table 4.1.1, the value of a follows linear regression with a slope of 0.021 and an intercept of 0.75. Therefore, the coefficient is calculated by means of equation (4.1.1).

$$a = 0.021m + 0.75 \tag{4.1.1}$$

From figures 4.1.2, 4.1.3, 4.1.4 and 4.1.5 it can be observed how the primary vortices are more stable (figures on the right) with greater values of a. Also, it is appreciated that as the number of nodes is increased this linear

relation gives less accurate values of the distance. Figure 4.1.6 shows the position of the sheet of vortices for the value of the coefficient calculated with equation (4.1.1), confirming that the prediction done by the linear regression is less accurate for greater nuber of nodes.
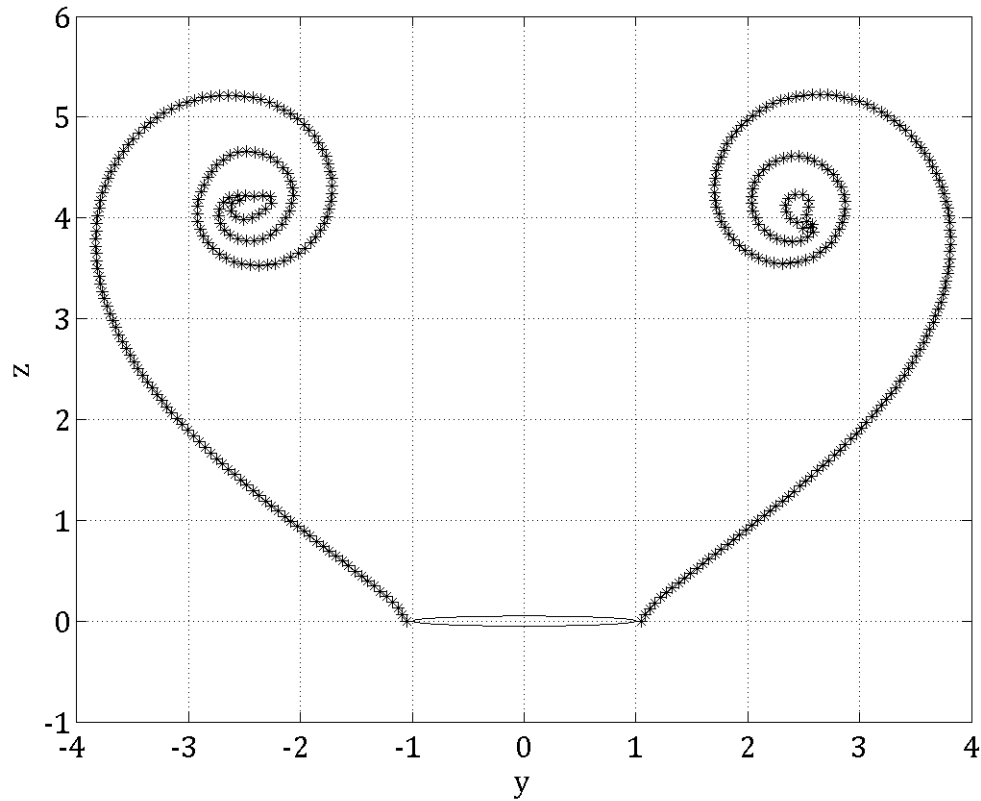

Figure 4.1.6: Shape of the sheet of vortices for $m = 1000$ at $t = 6$.

The last numerical parameter is the minimum distance (D_{min}) to construct the circulation line at the core of the vortex, a procedure that is explained in section 4.2. It gives the condition for the vortices which get very close inward the primary vortex to merge into one single vortex, to avoid what happens at the end of the sheet, what it is observed on Figure 4.1.6. After some simulations performed under the same conditions used up to now it has been observed that the simplification starts to work if D_{min} is above 0.08, and for values greater than 0.2 calculations do not hold. A good range of values has been proven to be [0.09, 0.15].

When choosing any of these numerical parameters it should be kept in mind that the calculations may be very sensitive to variations and solutions may decompose

Unless something different is specified in a particular case, to find results the parameters chosen are the ones on Table 4.1.2.

m	b	c	d_{att}	d_{mov}	d_v	D_{min}	Δ_t	t
600	1	0.05	0.05	$0.5 + i0.001$	$(0.021m + 0.75)D$	0.14	0.01	8

Table 4.1.2: Standard conditions used for calculations.

4.2   Circulation line simplification

In section 1.2 the evolution of the fluid on the surface of the wing was explained. Up to know, calculations are limited to short times, as when time goes on, the vortices agglomerate on the inside of the primary vortex sheet. This may lead to the sheet crossing itself or changing drastically direction, leading to non-physical solutions.

The way to deal numerically with this problem consists in placing a line of circulation that goes through the middle of the primary vortex, at the vortex core (see Figure 4.2.1). In a two dimensional plane this line is seen as a vortex.
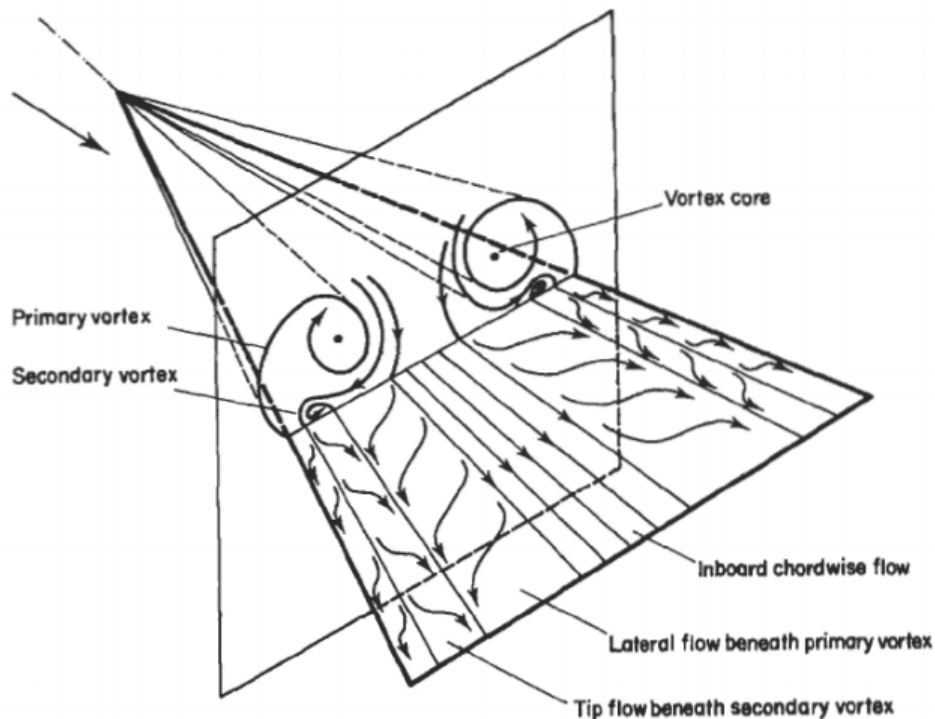

Figure 4.2.1: Schematic representation of the cross-section of the vortices generated over a delta wing.

As vortices are created near the leading edge, they go far from the profile. The first moving vortex of the sheet is the one that is taken as the primary vortex core, as the sheet rolls up on it. When the vortices get close to this vortex they merge with it and become one single vortex, whose circulation and position is the mean of their circulations and positions. This happens when the distance is smaller than a given distance (D_{min}), which is one of the numerical parameters of the problem, as it was explained on section 4.1.

Figure 4.2.2 shows the difference on the evolution of the vortex sheet between the case when the circulation line simplification is applied or not (both solutions in standard conditions). When the circulation is concentrated, using circulation line simplification, it can be noticed that the stability of the primary vortices is kept, the sheet rolls up without crossing itself and the vortices. Meanwhile, when the sheet rolls up freely, vortices are less stable and may cross themselves at some point. It should be also observed that in figure 4.2.2a the primary vortices rotate closer to the wing than in figure 4.2.2b.
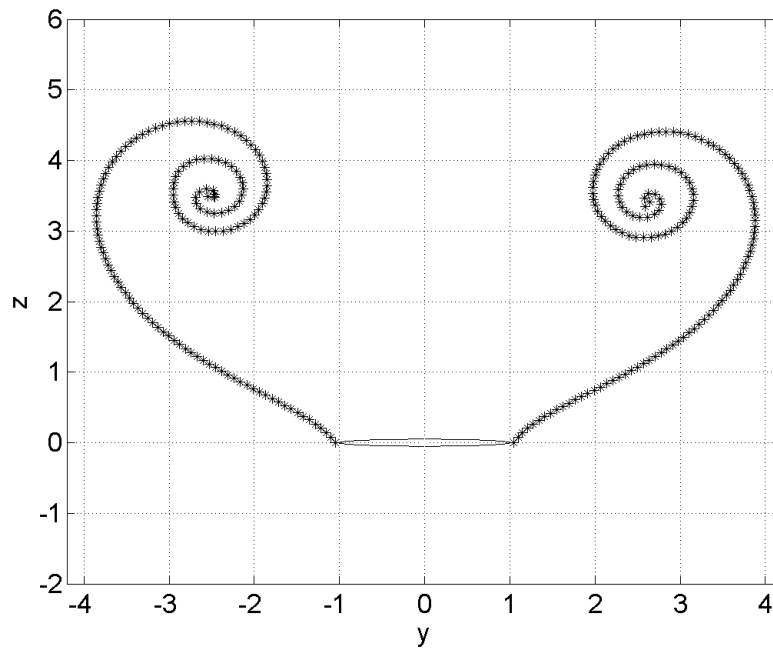
(a) With line vortex simplification.
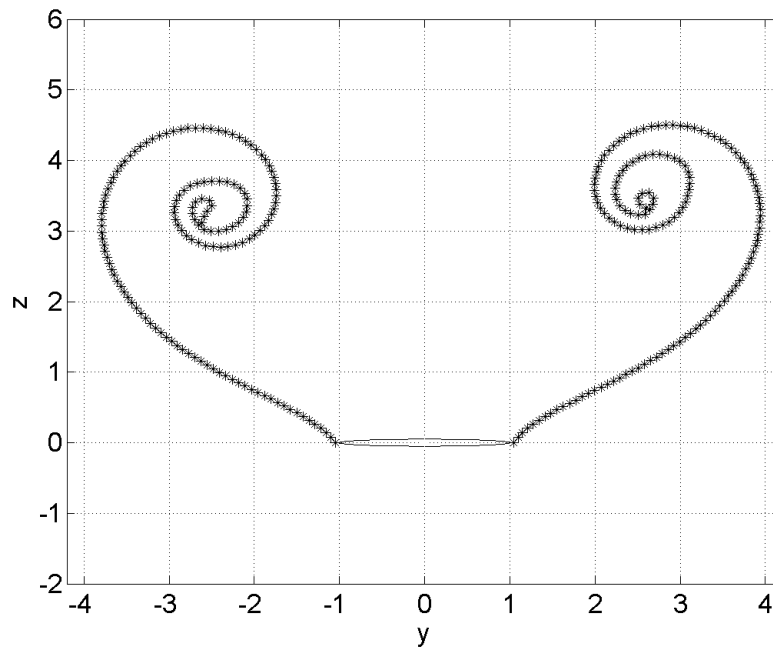
(b) Without line vortex simplification.

Figure 4.2.2: Evolution of the sheet of vortices at $t = 5$.

4.3 Pressure and lift coefficient

The pressure and lift coefficients are part of the characteristics of the aerodynamics of a wing. Several analyses regarding the pressure distribution over a delta wing ([6, 7]) have been developed, studying the lift in some particular cases. In [6] the difference between the value of the lift obtained by means of linearized potential theory and the experimental one is commented. The difference from one to the other is what is called the vortex lift, e.g. the lift generated by the vortices.

The pressure distribution on the lower surface of a delta wing follows an almost constant distribution. On the upper surface the pressure is only constant at the center of the wing. However, at the tips the primary vortices generate a suction peak increasing the velocity of the fluid and decreasing the pressure at the upper surface. Figure 4.3.1 shows for the same configuration (standard conditions), the evolution of the pressure coefficient (Cp) for three different time steps.
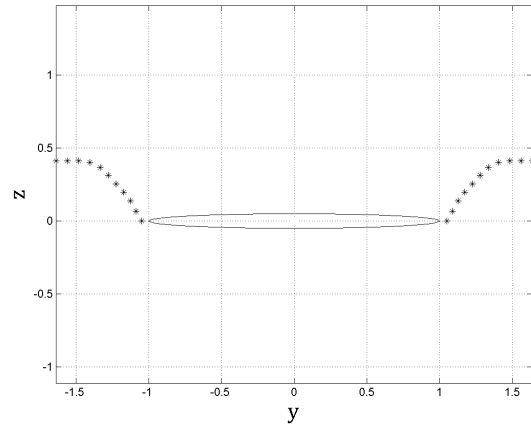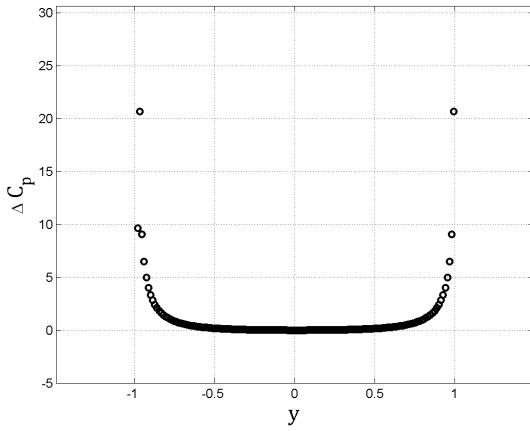
(a) Cp and position of the vortices in the sheet as a function of y at instant $t = 0.1$
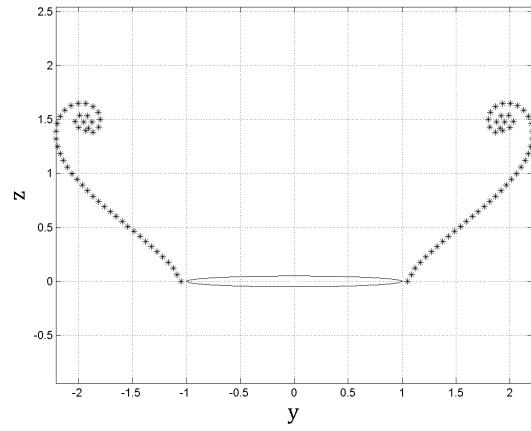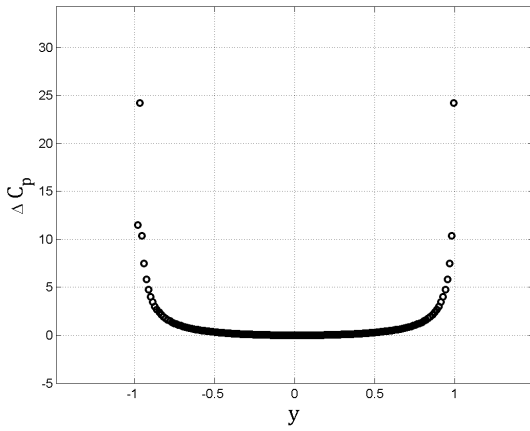
(b) Cp and position of the vortices in the sheet as a function of y at instant $t = 1$
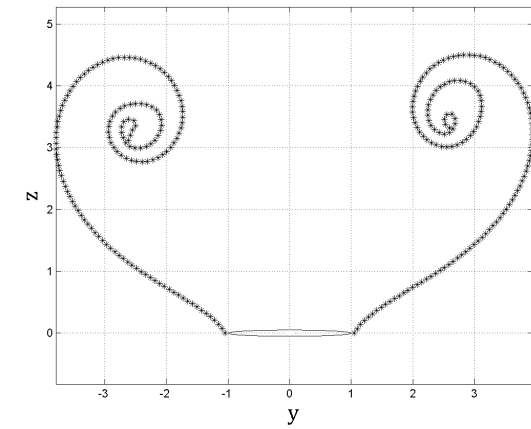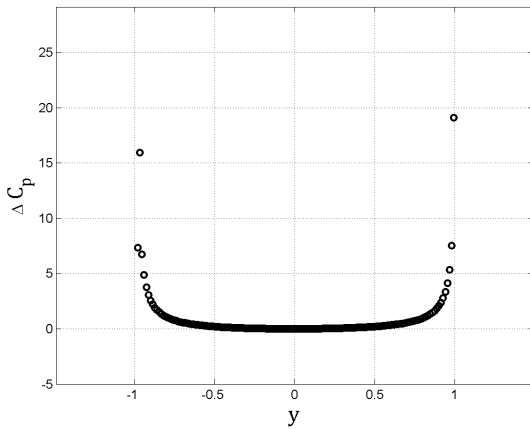
(c) Cp and position of the vortices in the sheet as a function of y at instant $t = 5$

Figure 4.3.1: Pressure coefficient (Cp) and shape of vortex sheet for different time steps.

It can be observed an increment on Cp between Figure 4.3.1a and Figure 4.3.1b due to the acceleration of the fluid produced by the generation of the primary vortices, which are sketched on the right panels of these figures. At a later time, Figure 4.3.1c shows how the pressure coefficient decreases as primary vortices go far from the wing. From this last figure it is also worth mentioning that the generation of the vortices that form the sheet develops a small anti-symmetry with time, dealing to anti-symmetric distributions of the flow.

Regarding the lift coefficient, it varies with time as the vortex moves. At the beginning it takes a few instants for the vortex sheet to stabilize. During this time variations, on the lift coefficient are considerably high .The lift coefficient reaches its maximum when the vortices reach a stability and then stars decreasing as the vortices go far from the profile. This evolution can be observed on Figure 4.3.2. The lift of the wing corresponding time instants configurations of Figure 4.3.1 is represented on Figure 4.3.2 by triangles and its values are: $C_l = 0.9044$ for $t = 0.1$, $C_l = 1.2375$ for $t = 0.1$ and $C_l = 0.8390$ for $t = 0.1$.
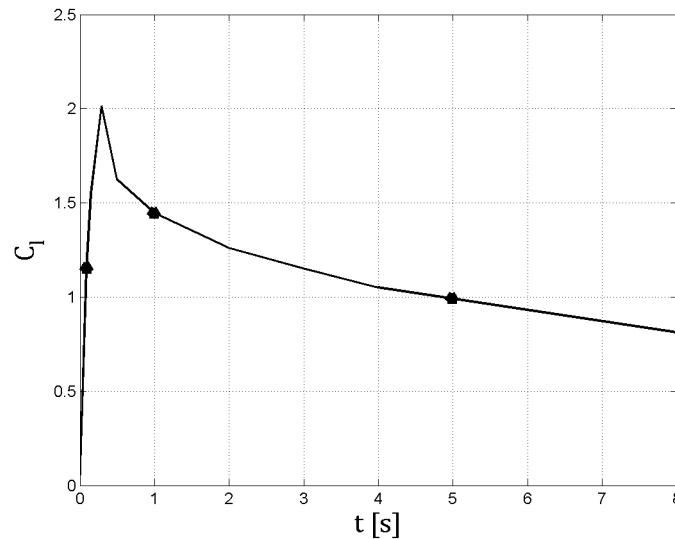

Figure 4.3.2: Evolution of the lift coefficient (C_l) with time

4.4 Thickness effect

Previous works have developed numerical methods which closely approximate the normal-force characteristics of a plane delta wing ([8]). The purpose now is to start looking into the effects of thickness on this kind of wing configuration.
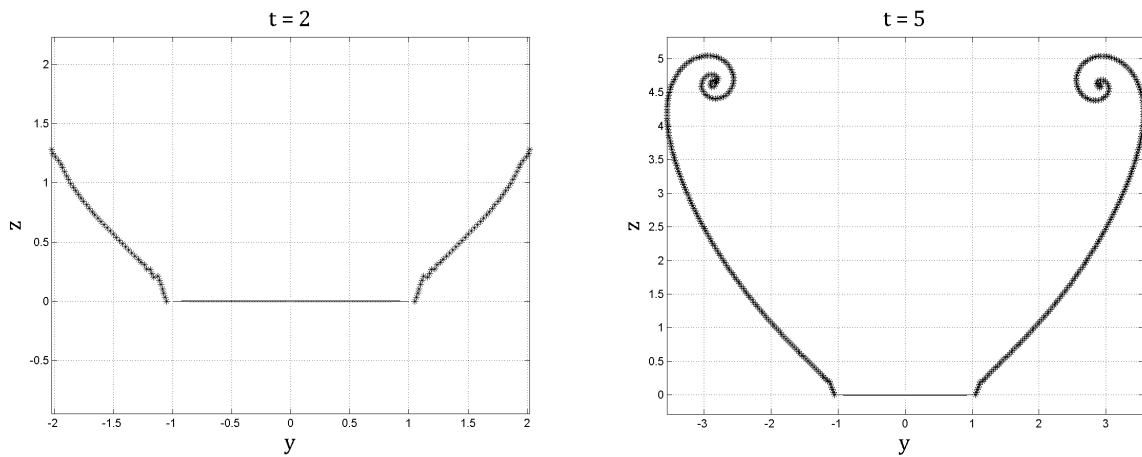
To see how vortices behave in presence of a wing with thickness, some simulations are carried out under standard conditions, but with different values of the thickness (c).
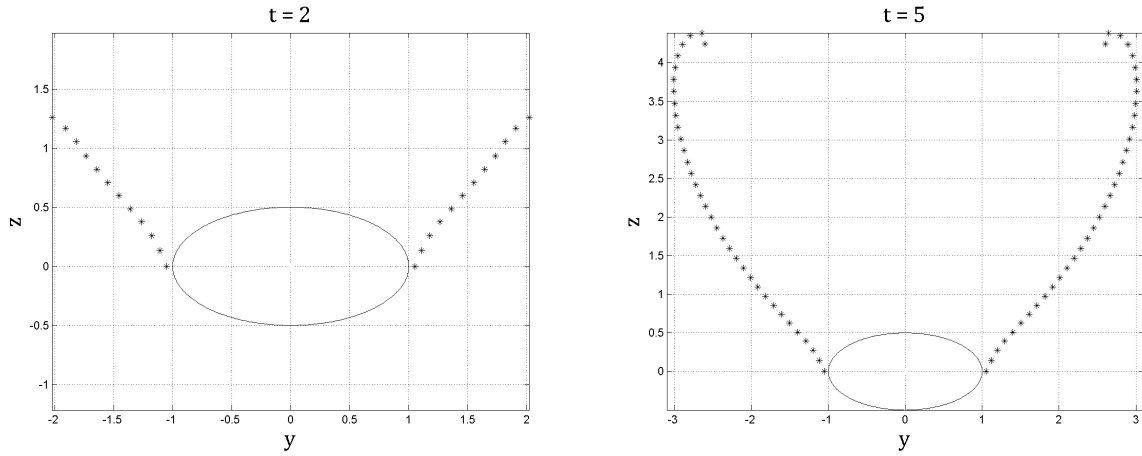
(a) Position of the vortices with $c = 0.5$
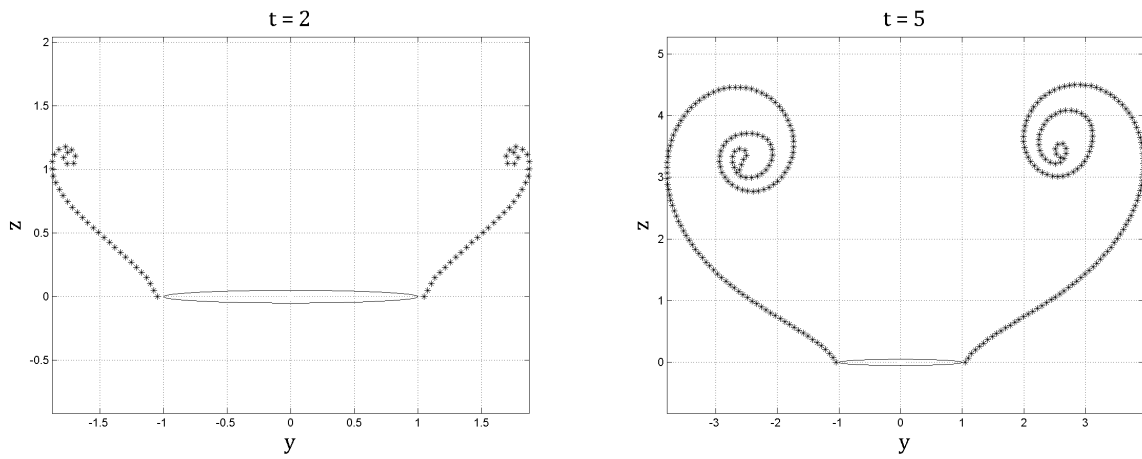
(b) Position of the vortices with $c = 0.05$

(c) Position of the vortices with $c = 0.005$

Figure 4.4.1: Position of the sheet of vortices at $t = 2$ and $t = 5$ for different wing thickness.

Figure 4.4.1 shows how the sheet of vortices behaves for different thickness. The time steps are shown for each case. In the case where the wing is thicker (Figure 4.4.1a) the sheet goes faster from the profile than in the other two cases, while the rolling up of the sheet takes longer times. When the thickness of the wing is reduced one order of magnitude (Figure 4.4.1b) the vortices lose vertical velocity and the rolling up of the sheet starts at very early times. If the thickness is decrease another order of magnitude the flow is made more slender, the fluid goes faster and the radius of the rolling up of the sheet is smaller.

Chapter 5

Conclusions

The physics involved in the aerodynamics of delta wings is very complex, some assumptions have been made to reach a first approximate solution to the behavior of a fluid in presence of a delta wing. The solutions given by this code are a small insight on the aerodynamics of a delta wing.

One of the strongest assumptions that is made are the values given to the numerical parameters of the problem. These values have been chosen by trial and error, until an acceptable combination has been found. In some of them, like the panel size (i.e. number of nodes or panels), comparisons with analytical solutions have been done to ensure that the values are appropriate. However, in others, such as the distance of the attached vortices, etc. no comparison with analytical solution was possible. However, this choice is made at a guess and it has not been verified. To have more reliable results, experimental analysis or comparison with other simulation techniques would be needed.

Also, it has been observed that solutions for long times can't be obtained as the vortex sheet becomes unstable. Boundary-element methods are usually quite unstable, so different smoothing techniques are used. In the present paper, some of them are used (i.e. uniform spacing between the vortices of the sheets), although more sophisticated techniques are obviously needed. Figure 5.0.1 shows what happens when equations do not hold. The vortices that shape the sheet start to concentrate near the leading edge and provoke the disappearance of the sheet. It has to be pointed out that a stationary solution can't be obtained from this analysis, since it does not hold for long times.
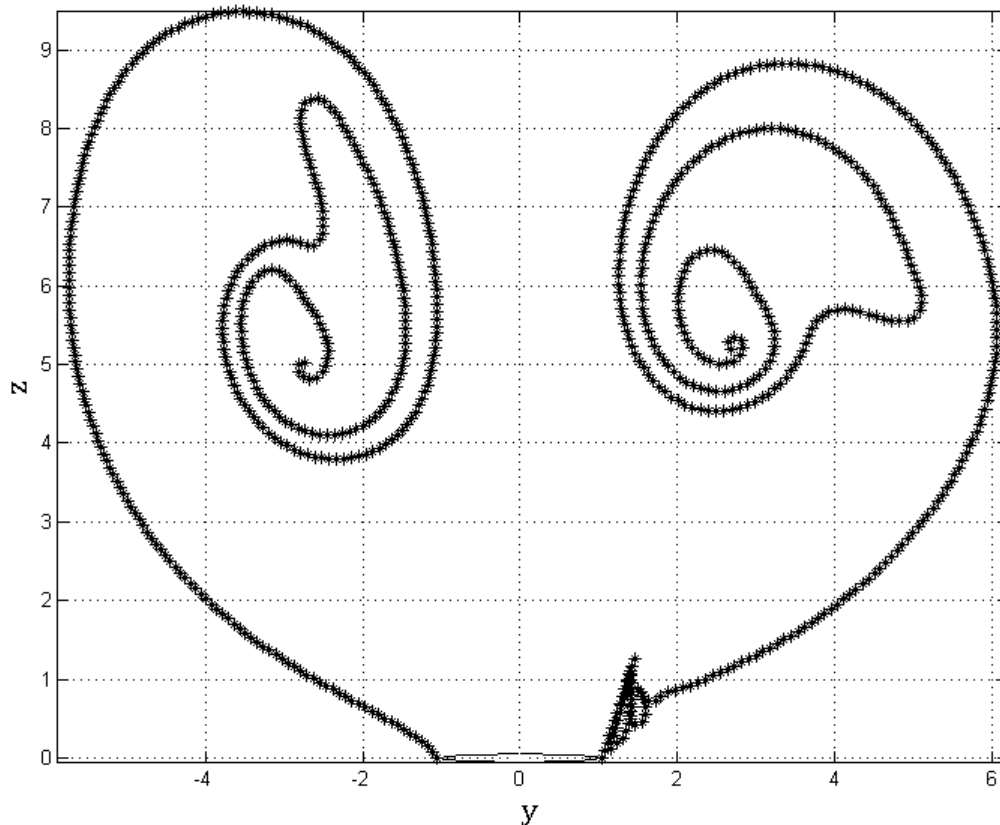
Figure 5.0.1: Shape of the sheet of vortices for $t = 10$, at standard conditions.

Moreover, for the objective of this study, the viscous effects that take place at the wall of the wing are not taken into account. Considering the viscous solution, the suction peak is lower than the one calculated by an inviscid approximation and there is not a fully pressure recovery once the separation has taken place (simulations on the effect of boundary layer separations have been carried out by Kirkköprü and Riley [9]). Assuming an inviscid problem, solutions obtained for lift and pressure distribution are ideal but far from being realistic.

It can be concluded that the code developed to compute numerically the sheet of vortices that rolls-up over a delta wing flying in an incompressible flow gives suitable results.

Further investigations can be carried out developing this project. For instance, the effect of the cross wind and its consequences on the stability of the aircraft can be studied. Also viscous effects and secondary separation of the boundary layer can be included in the simulations.

Bibliography

[1] *Development of Aviation Technology, Delta wings.* Available at: http://www.century-of-flight.net/Aviation%20history/evolution%20of%20technology/Delta%20Wings.htm.

[2] Dowling, Stephen. *A handful of British Spitfire pilots cheated death in high-speed dives that helped pave the way towards supersonic flight.* Available at: http://www.bbc.com/future/story/20160505-the-spitfires-that-nearly-broke-the-sound-barrier.

[3] Hallion, Richard P. *Supersonic Revolution.* Available at: http://www.historynet.com/supersonic-revolution.htm.

[4] Anderson, Jr. John D. *Fundamentals of Aerodynamics (3rd edition).* McGraw-Hill. New York, 2001.

[5] Gordillo Arias de Saavedra, Jose Manuel and Riboux Acher, Guillaume. *Introducción a la Aerodinámica Potencial.* Ediciones Paraninfo, S.A, 2012.

[6] Katz, Joseph. Plotkin, Allen. *Low Speed Aerodynamics - From Wing Theory to Panel Methods.* McGraw-Hill, 1991.

[7] Kirkpatrick, ,D.L.I., *Analysis of the Static Pressure Distribution on a Delta Wing in Subsonic Flow.* Aerodynamics Dept., R.A.E., Farnborough, 1970.

[8] *Smith, J.H.B., Improved Calculations of leading edge Separation from Slender, Thin, Delta Wings.* Royal Aircraft Establishment, Farnborough (1968)

[9] Kirkköprü, K. and Riley, N. *Laminar-flow Secondary Separation on a Slender Wing.* University of East Anglia, Norwich (United Kingdom), 1991.

[10] Riley, N. *Separation from a smooth surface in slender conical flow.* Journal of Engineering Mathematics, 1979.